Hindawi
International Journal of Antennas and Propagation
Volume 2022, Article ID 1270271, 10 pages
https://doi.org/10.1155/2022/1270271

Research Article

A Cloud-Structured Fractal Multiband Antenna for 4G/5G/WLAN/Bluetooth Applications

Zhen Yu, Guodong Zhang, Xiaoying Ran, Ziheng Lin, and Yao Li

North China Institute of Science and Technology, Langfang 101601, China

Correspondence should be addressed to Xiaoying Ran; starsky202@ncist.edu.cn

Received 10 June 2022; Accepted 21 September 2022; Published 11 October 2022

Academic Editor: Muhammad Zubair

This study proposes a multiband printed planar antenna with cloud-like grooves. The outer contour of the antenna is shaped like a cloud, and the groove-like pattern is similar to the cloud-like pattern in ancient China. It can support 3G, 4G, 5G, WLAN, Bluetooth, WiMAX, and other applications. Based on the traditional monopole antenna, the antenna combines the advantages of a coplanar waveguide. The antenna uses an Archimedes helix to create grooves that resemble ancient Chinese cloud structures. Three effective frequency bands are obtained. The relative bandwidth of the first frequency band (1.8–2.6 GHz) is 32.7%, covering 5G band n2 (1.85 GHz–1.99 GHz), WCDMA (1.9–2.17 GHz), LTE33-41 (1.9–2.69 GHz), Bluetooth (2.4–2.48 GHz), WLAN (2.4–2.48 GHz), LTE Band40 (2.3–2.4 GHz), ISM Band (2.42–2.4835 GHz), WiMAX (2.3 GHz), and SCDMA (1.88–2.025 GHz and 2.3–2.4 GHz). The second frequency band (3.35–4.1 GHz) has a relative bandwidth of 20.5%, covering LTE42/43 (3.4–3.8 GHz) and 5G band n78 (3.4 GHz–3.8 GHz). The relative bandwidth of the third band (5.5–7.9 GHz) is 40.3%, covering Emergency and Public Protection (5.85 GHz–5.925 GHz) (WRC03). The antenna is printed on a G10/FR4 dielectric board with a size of $1.6 * 45 * 40\,\text{mm}^3$, the dielectric constant is 4.4, and the omnidirectional radiation pattern gain is 0.59–4.14 dBi. The measurement results are in good agreement with the simulation results. The proposed design method is verified to meet the requirements of various wireless applications.

1. Introduction

With the wide application and development of radio, the demand for different antennas is also increasing, and the antenna performance requirements are getting higher and higher. In recent years, multiband and miniaturized antennas have become hot spots for mobile terminal equipment [1]. Due to the inherent characteristics of traditional monopole and dipole antennas, it is challenging to meet the practical requirements of miniaturization and multiband, so coupling feeding technology [2–4], fractal technology [5], matching network loading technology [6], and fractal techniques [5] to meet the relevant requirements for antenna performance. In addition, different feeding methods will also have a particular impact on the antenna's performance. For example, although the microstrip line feed mode has excellent antenna performance, its bandwidth is relatively narrow [7–9]. Coplanar waveguides have higher conductor losses than microstrip lines, although they have a wider frequency bandwidth and impedance range.

Antennas can also improve antenna performance by nesting a simple graph for multiple iterations and self-similarity [10, 11]. This method enables the antenna to have similar surface currents at different positions of the radiator, space-filling [12, 13], reducing the size of the antenna and making the antenna more compact and flexible. The antenna's performance can also be improved by making slots of different shapes in the antenna radiator.

In [14], the authors summarize the design idea of combining antenna fractal and slotting techniques. The antenna's performance can be considered while realizing multifrequency bands through the slotting and fractal design of the circular monopole patch. In [15], the authors used coplanar waveguide antennas to widen the frequency band. In [16] the authors discussed the interference of the external environment on each frequency band. Among them, the

frequency band below 6 GHz has strong distortion immunity and penetrating ability to buildings because of the longer wavelength. And the frequency band below 6 GHz can meet the vast majority of communication needs. Therefore, controlling the antenna coverage frequency band below 6 GHz helps to improve the robustness of the antenna system. In [17], the authors designed the reference ground plane of the coplanar waveguide to be a semielliptical shape. They proposed the design of helical grooves on the ground plane to expand the bandwidth while meeting the performance requirements of multiple frequency bands. In addition, many other methods are used in antenna design, such as the Cartesian curve, the Sierpinski triangle type, the Koch curve type, and so on.

It has been shown that the frequency band of an antenna can be increased by adding branches and slits [18, 19]. Therefore, to avoid the poor antenna bandwidth and performance caused by the characteristics of traditional monopole or dipole antennas, an antenna with better performance and wider bandwidth can be designed, which can effectively combine the above technologies.

In this paper, a multiband antenna with a cloud-like structure is proposed, and the antenna radiator is slotted with an Archimedes spiral structure, and the groove structure is similar to the traditional Chinese cloud-like structure. Slotting has three fractal iterations. The commercial frequency bands covered by the antenna include 5G band n2 (1.85 GHz–1.99 GHz), WCDMA (1.9–2.17 GHz), LTE33-41 (1.9–2.69 GHz), Bluetooth (2.4–2.48 GHz), WLAN (2.4–2.48 GHz), LET band40 (2.3–2.4 GHz), ISM band (2.42–2.4835 GHz), WiMAX (2.3 GHz), SCDMA (1.88–2.025 GHz and 2.3–2.4 GHz), LTE42/43 (3.4–3.8GHZ), WiMAX (3.3–3.8GHZ), 5G band n78 (3.4 GHz–3.8 GHz), and Emergency and Public Protection (5.85 GHz–5.925 GHz) (WRC03). Compared with [14], the antenna proposed in this paper has a larger bandwidth and higher radiation efficiency.

2. Antenna Structure and Design Procedure

2.1. Characteristics of the Antenna Structure. The formula for calculating the relationship between antenna frequency and electrical length is

$$f = \frac{c}{2L\sqrt{\varepsilon_r}}, \tag{1}$$

where L is the electrical length of the antenna radiator, f is the frequency at the center frequency of the antenna, c is the speed of light in free space ($3 * 108$ m/s), and ε_r is the dielectric constant of the dielectric substrate

The structure of the coplanar waveguide antenna proposed in this study is shown in Figure 1, and its dimensions are shown in Table 1. An arc-shaped 50 Ω coplanar waveguide feeders is used to extend the bandwidth. The antenna has three iterations of cloud structure grooves similar to the fractal structure of ancient Chinese cloud-shaped ornaments, as shown in Figure 2. The cirrus pattern used for this coplanar waveguide antenna first appeared in the pre-Qin period in China. It is the source of all the cloud patterns in

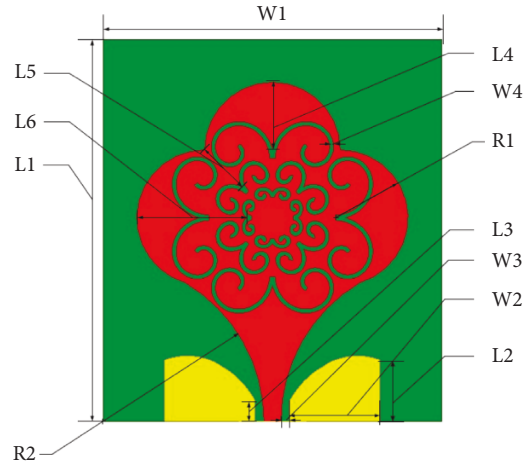

Figure 1: Antenna structure layout.

Table 1: The dimensions of the proposed antenna design.

Dimensions parameters	$L1$	$L2$	$L3$	$L4$	$L5$	$L6$
Unit(mm)	45	7.3	2.5	7.9	6	13
Dimensions parameters	$W1$	$W2$	$W3$	$W4$	$R1$	$R2$
Unit(mm)	40	10.7	1	0.5	8	19

(a) (b)

Figure 2: (a) Cloud pattern jade wall of the Tang dynasty. (b) Tile-end with rolling cloud design warring states period.

ancient China, representing auspiciousness, joy, and happiness and revealing the ancient Chinese people's yearning for a better life. As the representative of ancient Chinese traditional auspicious patterns, the cloud pattern is a unique representative of Chinese cultural symbols. It has profound cultural connotations, rich and complex symbolic meanings, and artistic sense. More importantly, this structure can increase the length of the radiator, thereby increasing the antenna's electrical length and radiation efficiency.

The antenna was fabricated on an FR-4 substrate with a thickness of 1.6 mm, a dielectric constant of 4.4, and a loss tangent of 0.02. The basic geometry of ancient cloud structure fractal antennas is a cloud structure monopole with a helical slot. The formula for the Archimedes spiral structure is

$$\begin{aligned} X(\_t) &= 0.001 * \exp(0.21 * (\_t)) * \cos(\_t), \\ Y(\_t) &= 0.001 * \exp(0.21 * (\_t)) * \sin(\_t), \end{aligned} \tag{2}$$

(a) (b)

Figure 3: (a) Archimedes spiral structure; (b) cloud-like structure.

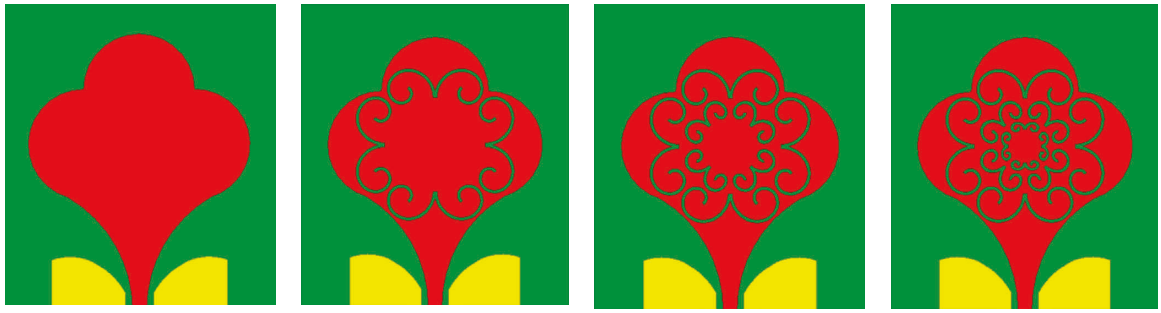

(a) (b) (c) (d)

Figure 4: Iterative process of antenna: (a) 0 iterations, (b) 1st iteration, (c) 2nd iteration, and (d) 3rd iteration.

(a) (b)

Figure 5: Evolution process of grounding plane. (a) Before the evolution. (b) After the evolution.

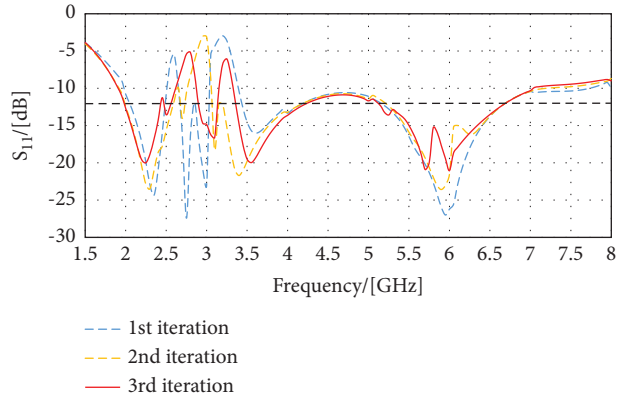

Figure 6: S11 comparison diagram of antenna iteration.

where the initial value of _t is 0, end value of _t is 2.35 ∗ pi, and width is 0.5 mm. The first-order Archimedes spiral model obtained by the formula is rotated by −45° to obtain the structure shown in Figure 3(a). The cloud-like structure shown in Figure 3(b) is obtained by mirror copying the structure of Figure 3(a).

As shown in Figure 4, three iterations were performed to achieve a multiband response. In the evolution of the ground plane, the top of the trapezoidal ground plane is combined with the arc to obtain the ground plane model in this design.

The three positioning points of the arc are (−15.2, 12.5, 0), (−20, 2, 0), and (−15.5, 6.8, 0). The evolution path is shown in Figure 5.

The fractal formula of the cloud-like groove structure can be simply expressed as follows:

$$D_n = \left(\frac{1}{2}\right)^n D_1. \tag{3}$$

Here, "D_n" represents the nth order fractal

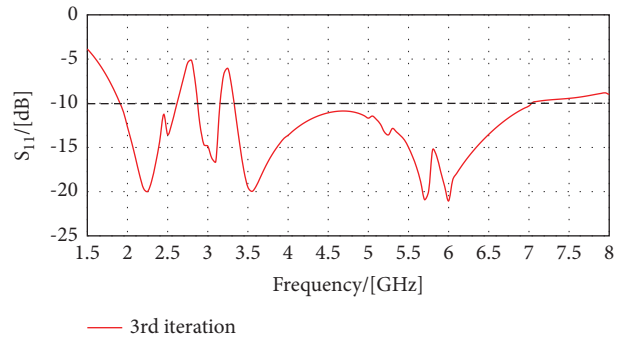

Figure 7: The S11simulation value of the final antenna model.

The corresponding electrical length of the antenna at low frequencies can be calculated as follows:

$$L_a = \frac{1}{2}D_1 + \frac{5}{12}\pi R_2 \approx 33.8\text{mm}, \tag{4}$$

Table 2: Simulated frequency bands covered by the antenna.

Band no.	Bandwidth	Covered commercial bands
1	1.9–2.6 GHz (29%)	5G band n2 (1.85 GHz–1.99 GHz) WCDMA (1.9–2.17 GHz) LTE33–41 (1.9–2.69 GHz) Bluetooth (2.4–2.48 GHz) WLAN (2.4–2.48 GHz) LTE band40 (2.3–2.4 GHz) ISM band (2.42–2.4835 GHz) WiMAX (2.3 GHz) SCDMA (1.88–2.025 GHz, 2.3–2.4 GHz)
2	2.9–3.15 GHz (8%)	None
3	3.35–7 GHz (72%)	LTE42/43 (3.4–3.8 GHz) WIMAX (3.3–3.8 GHz) 5G band n78 (3.4 GHz–3.8 GHz)WLAN (5.15–5.35 GHz) Emergency and Public Protection (5.85 GHz–5.925 GHz) (WRC03)

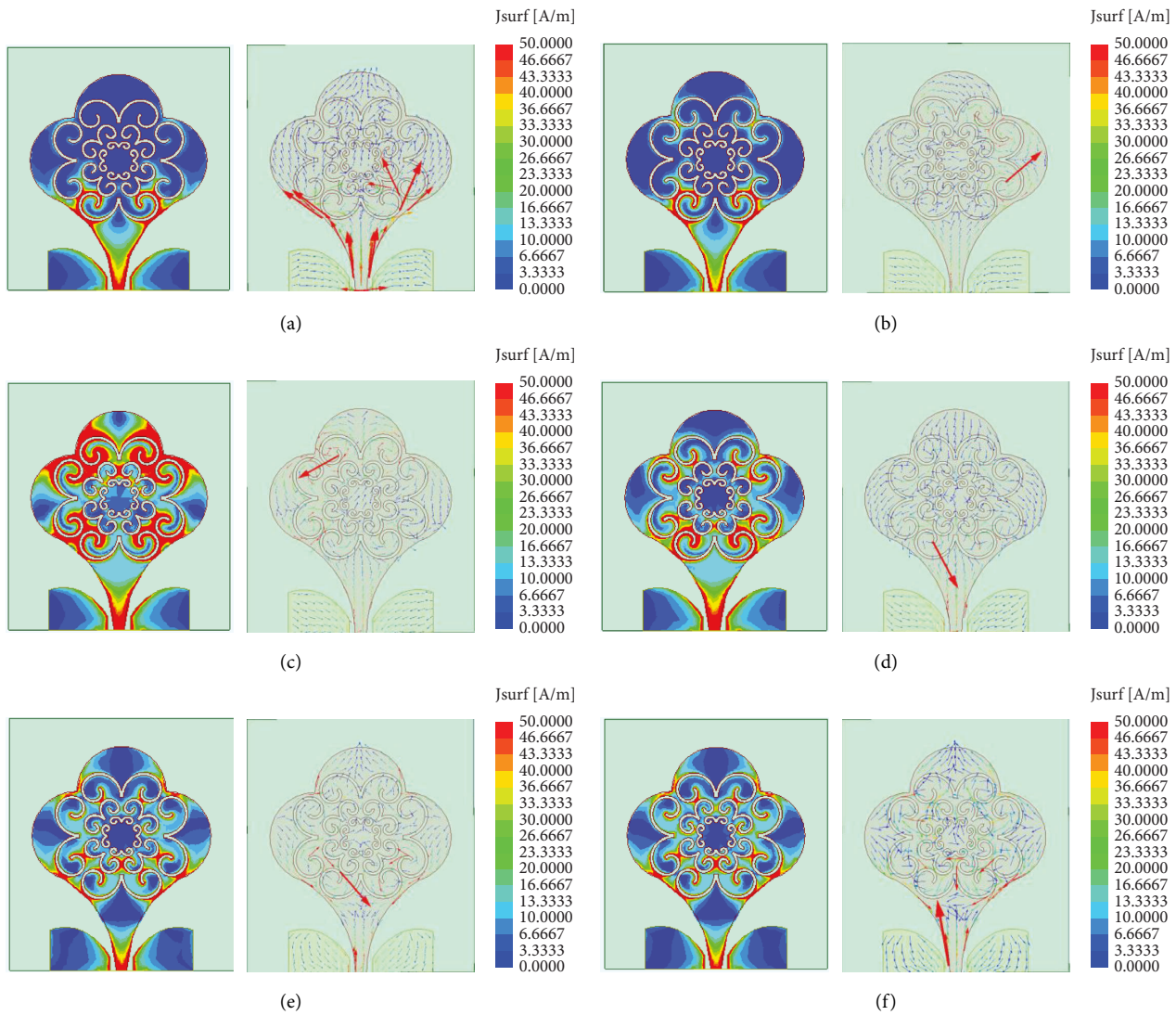

Figure 8: Current amplitude and vector distribution of the antenna at (a) 2.25 GHz, (b) 2.5 GHz, (c) 3.1 GHz, (d) 3.55 GHz, (e) 5.7 GHz, and (f) 6 GHz.

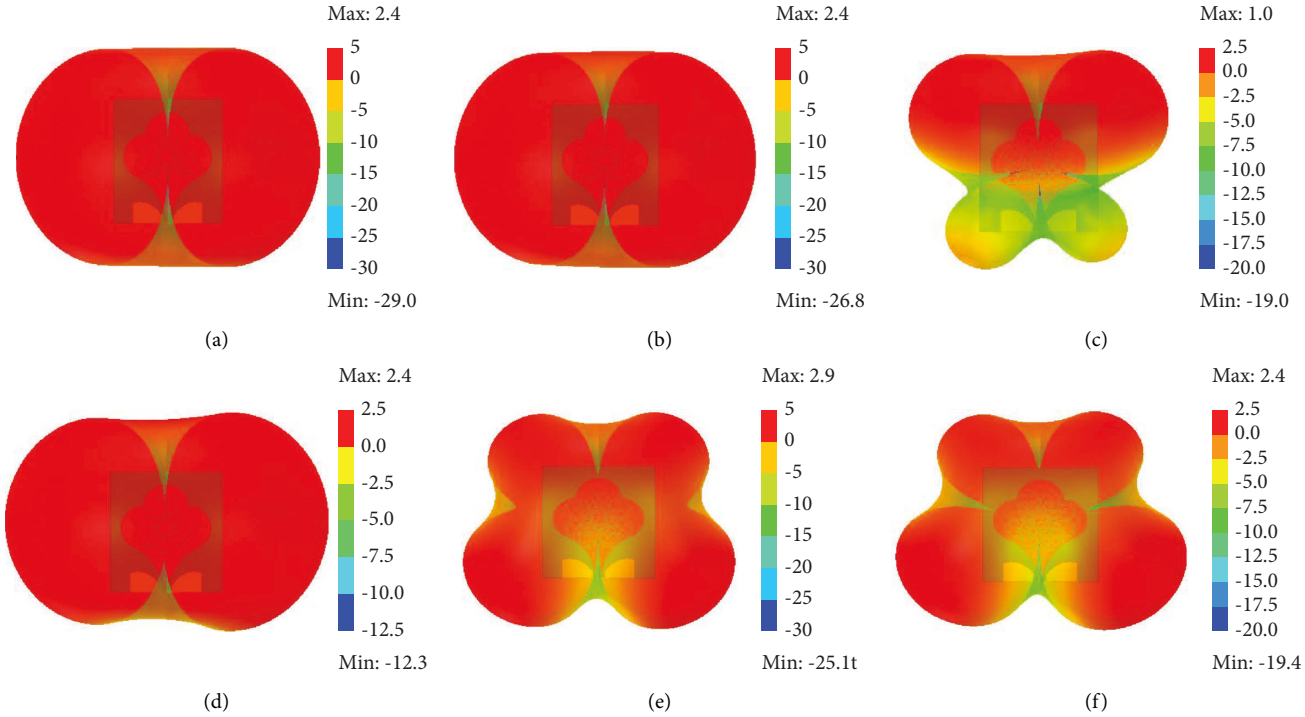

Figure 9: 3D radiation patterns at (a) 2.25 GHz, (b) 2.5 GHz, (c) 3.1 GHz, (d) 3.55 GHz, (e) 5.7 GHz, and (f) 6 GHz.

calculated by the following formula:

$$f_{\text{low}} = \frac{c}{2L_a\sqrt{\varepsilon_r}} \approx 2.22\text{GHz}. \tag{5}$$

The corresponding electrical length of the antenna at high frequencies can be calculated as follows:

$$L_b = \frac{1}{2}D_1 + \frac{1}{3}D_2 \approx 12.67\text{mm}, \tag{6}$$

calculated by the following formula:

$$f_{\text{high}} = \frac{c}{2L_b\sqrt{\varepsilon_r}} \approx 5.92\text{GHz}. \tag{7}$$

3. Simulation Results

The ANSYS Electronics Desktop (HFSS) (Version 20) software package was used for the simulation. The basic model of the antenna can be regarded as a monopole antenna with a capacitive load similar to a cloud-shaped structure. The first-order radiator is formed by etching the cloud structure groove with the Archimedes spiral structure as the initial pattern evolution on the radiator. Model and generated five central resonance frequencies, which tended to stabilize as the number of iterations increased. Furthermore, it reaches the best at the third fractal iteration, which produces the center frequency we need. See Figure 6.

The antenna proposed in this paper can work in three frequency bands: the center frequencies are 2.25 GHz, 2.5 GHz, 3.1 GHz, 3.55 GHz, 5.7 GHz, and 6 GHz, respectively, and the corresponding S11 are −19.9 dB and −13.54 dB, −16.6 dB, −19.97 dB, −20.90 dB, −21.04 dB. The simulated −10 dB S11 relative bandwidth is 29% of the first band (1.9–2.6 GHz), 8% of the second band (2.9–3.1 GHz), and 72% of the third band (3.35–7 GHz), See Figure 7. These frequency bands cover commercial frequency bands such as 4G-LTE, WLAN, Bluetooth, WiMAX, public protection, emergency frequency bands, and 5G (see Table 2 for antenna radiators).

The surface current amplitude and vector distribution of the antenna radiator part are shown in Figures 8(a)–8f, respectively. With the increase of the frequency, the changing trend of the surface current distribution of the antenna is from the edge of the radiator and the first-order groove of the antenna to gradually spread to the second-order and third-order grooves. Among them, the surface current of the antenna is mainly distributed at the edge of the radiator and the first-order groove at the bottom at 2.25 GHz and 2.5 GHz, and the surface current of the antenna at 3.1 GHz and 3.55 GHz is mainly distributed between the first-order groove and the second-order groove. At 5.7 GHz and 6 GHz, the surface current of the antenna gradually spreads to the third-order groove. The overall trend is that the surface current of the antenna tends to concentrate towards the third-order groove as the frequency increases.

The peak gains are 2.4 dBi, 2.4 dBi, 1.0 dBi, 2.4 dBi, 2.9 dBi and 2.4 dBi at center frequencies of 2.25 GHz, 2.5 GHz, 3.1 GHz and 3.55 GHz, 5.7 GHz and 6 GHz, respectively. The simulated 3D far-field radiation pattern and the far-field normalized E/H surface radiation pattern are shown in Figures 9 and 10. It can be seen from Figure 9 that the omnidirectional performance of the antenna at each frequency point is good, but side lobes appear at 3.1 GHz, 5.7 GHz, and 6 GHz. It can be seen from Figure 10 that the

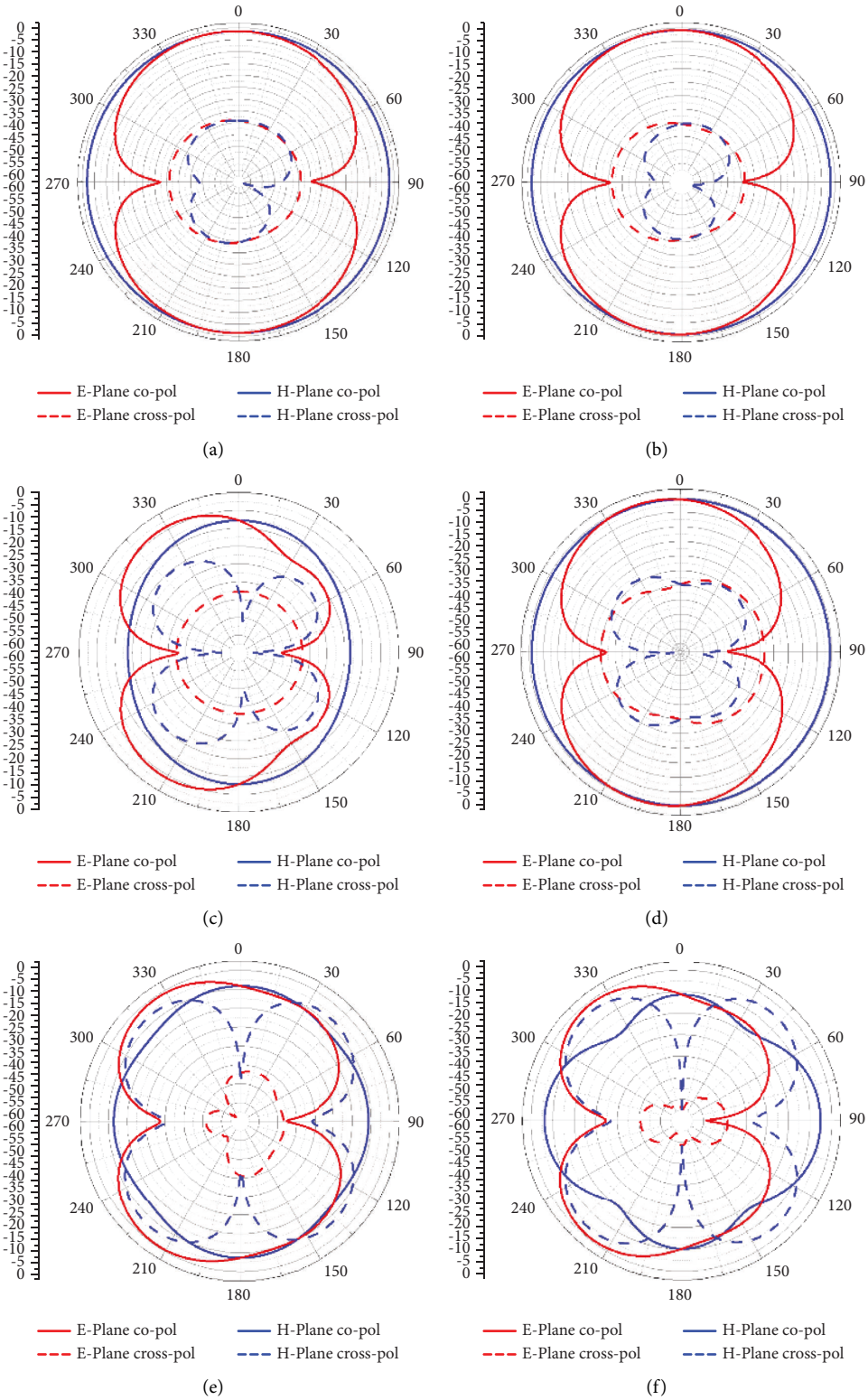

Figure 10: E- and H- plane radiation patterns at: (a) 2.25 GHz, (b) 2.5 GHz, (c) 3.1 GHz, (d) 3.55 GHz, (e) 5.7 GHz, and (f) 6 GHz.

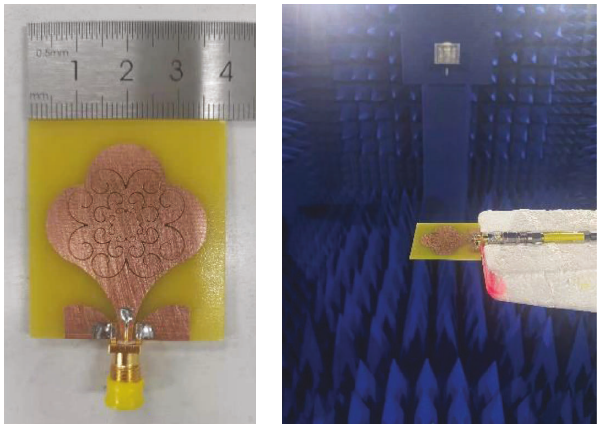

(a) (b)

Figure 11: (a) The antenna prototype. (b) The antenna is tested in an electromagnetically shielded darkroom.

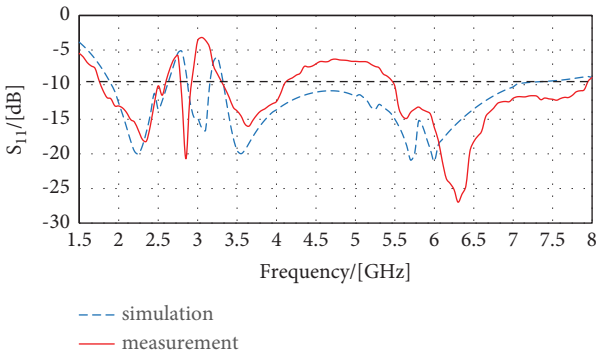

Figure 12: Comparison of antenna simulation and measurement.

overall degree of cross-polarization in each frequency band of the antenna is low. But as the frequency increases, the cross-polarization of the antenna gradually increases relative to the main polarization. However, the isolation degree of the overall cross-polarization from the main polarization is within an acceptable range.

4. Fabrication and Measured Results

The actual antenna was fabricated and tested to verify the correctness of the bandwidth, frequency, and performance in the design scheme. The antenna size is 45mm $*$ 40mm printed on a 1.6 mm thick Polytetra (G10/FR4) dielectric board. The dielectric constant of the dielectric plate is $\varepsilon_r = 4.4$ and the loss tangent is 0.02. The antenna has been placed into an electromagnetically shielded darkroom for testing (See Figure 11).

The actual antenna S11 obtained from the test is compared with the simulated S11, as shown in Figure 12. The first frequency point is shifted from 2.25 GHz to 2.35 GHz and its S11 value is −18 dB. The second frequency point is shifted from 2.5 GHz to 2.55 GHz and its S11 value is −11.9 dB. The S11 value of the third frequency shifted from 3.1 GHz to 2.85 GHz is −21.2 dB. The fourth frequency point is shifted from 3.55 GHz to 3.65 GHz and its S11 value is −15.5 dB. The fifth frequency shifted from 5.7 GHz to 5.6 GHz and its S11 value was −14.6 dB and the sixth frequency shifted from 6 GHz to 6.3 GHz and its S11 value was −27 dB. There are four frequency bands corresponding to the above frequency points, and the first frequency band (1.8 GHz–2.6 GHz) has a phase bandwidth of 32.7%. The relative bandwidth of the second frequency band (2.8 GHz–2.9 GHz) is 3.5%. The relative bandwidth of the third frequency band (3.35 GHz–4.1 GHz) is 20.5%. The relative bandwidth of the fourth frequency band (5.5 GHz–7.9 GHz) is 40.3%. There is little difference between the specific coverage application and the simulation, as shown in Table 3. The simulation results are in good agreement with the actual test results, but there are still some errors. The cause of the error may be related to the fabrication and welding process of the antenna.

Table 3: The frequency bands covered by the proposed antenna.

Band no.	Bandwidth	Covered commercial bands
1	1.8–2.6 GHz (32.7%)	5G band n2 (1.85 GHz–1.99 GHz) WCDMA (1.9–2.17 GHz) TE33-41 (1.9–2.69 GHz) Bluetooth (2.4–2.48 GHz) WLAN (2.4–2.48 GHz) LTE band40 (2.3–2.4 GHz) ISM band (2.42–2.4835 GHz) WiMAX (2.3 GHz) SCDMA (1.88–2.025 GHz and 2.3–2.4 GHz supplementary)
2	2.8–2.9 GHz (3.5%)	None
3	3.35–4.1 GHz (20.5%)	LTE42/43 (3.4–3.8 GHz), 5G band n78 (3.4 GHz–3.8 GHz)
4	5.5–7.9 GHz (40.3%)	Emergency and Public Protection (5.85 GHz–5.925 GHz) (WRC03)

Figures 13(a)–13(f) are the 3D far-field radiation pattern of the antenna at each frequency point and the comparison diagram of the main polarization and cross-polarization of the E/H plane of the antenna. It can be seen that as the frequency increases, the cross-polarization of the antenna gradually increases and the isolation gradually decreases, but the isolation of each frequency point of the antenna still meets the performance requirements of the antenna.

There are three effective frequency bands for the antenna: the first frequency band (1.8–2.6 GHz), the second frequency band (3.35–4.1 GHz), and the third frequency band (5.5–7.9 GHz). The gain and efficiency of the actual antenna are shown in Figure 14. As can be seen from the figure, the highest gain of the antenna reaches 4.56 dBi, and the maximum efficiency reaches 81%. In the effective frequency band of the antenna, the first frequency band gain range is 1.79–3.26 dBi, and the efficiency range is 45%–58%. The second band has a gain range of 0.59–2.92 dBi and an efficiency range of 71%–81%. The third-band gain is 1.27~4.14 dBi, and the efficiency is 55%~72%. This antenna can meet most application needs.

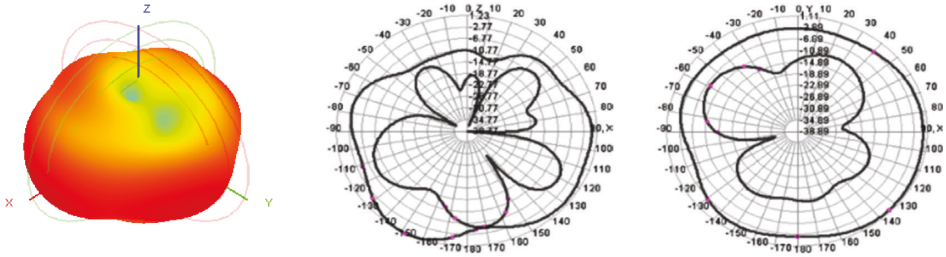

(1) (2) (3)

(a)

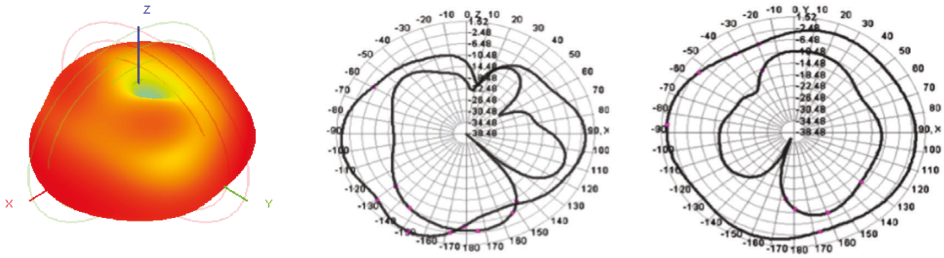

(1) (2) (3)

(b)

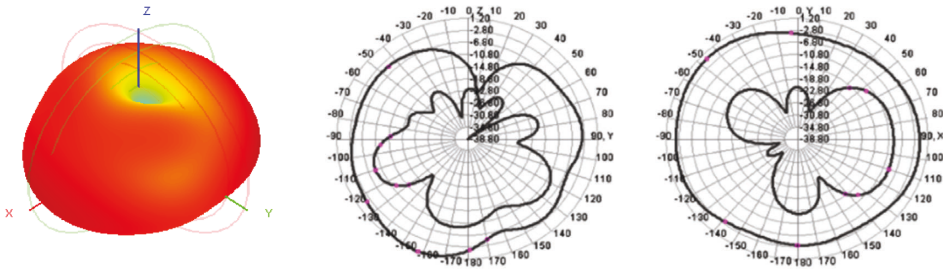

(1) (2) (3)

(c)

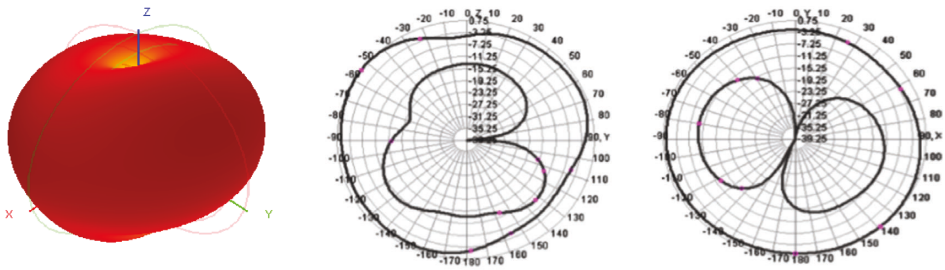

(1) (2) (3)

(d)

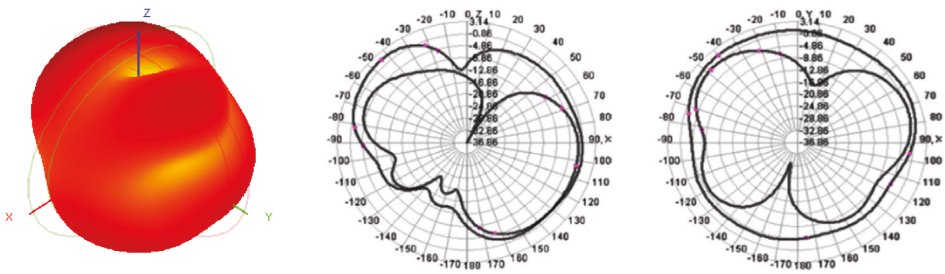

(1) (2) (3)

(e)

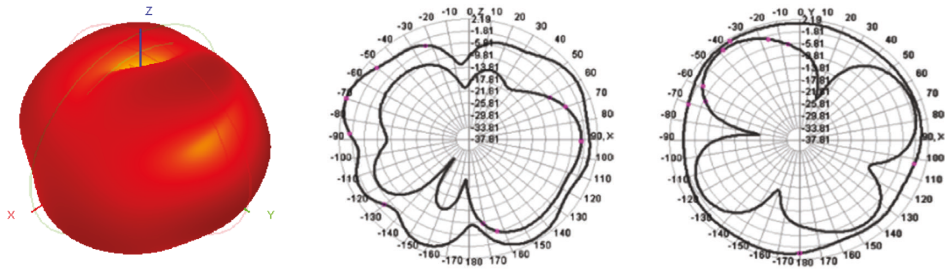

(1) (2) (3)

(f)

Figure 13: (1) 3D far-field radiation pattern of the antenna, (2) E-plane co-pol and cross-polarization comparison diagram, and (3) H-plane co-pol and cross-polarization comparison diagram; (a) 2.35 GHz, (b) 2.55 GHz, (c) 2.85 GHz, (d) 3.65 GHz, (e) 5.6 GHz, and (f) 6.3 GHz.

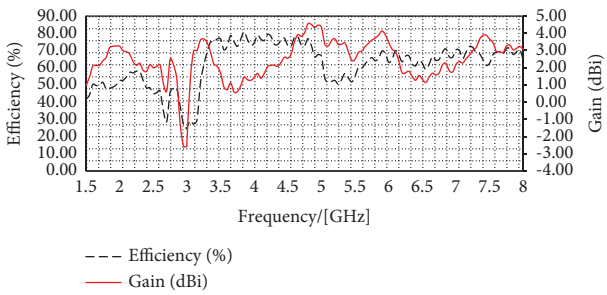

Figure 14: Gain and efficiency of antenna in measured state.

5. Conclusions

This paper develops a multiband coplanar waveguide antenna with a cloud structure for LTE, Bluetooth, WLAN, WiMAX, SCDMA, LTE42/43, and 5G. With a relative bandwidth of 41% (1.85–2.8 GHz), the first frequency band covers WCDMA, LTE33–41, Bluetooth, WLAN, LTE band40, ISM band, WiMAX, and SCDMA. In the second frequency band, the relative bandwidth is 17.94% (3.6–4.3 GHz), covering LTE42/43 and WiMAX, while the third frequency band, with a relative bandwidth of 38.55% (5.72–8.15 GHz), covers the 5G frequency band. According to the actual measurement of the antenna, the antenna gain in the frequency band below -10 dB is 0.59–4.14 dBi, and the antenna efficiency range is 28%–81%. Therefore, the antenna proposed in this experiment is suitable for most wireless applications due to its good radiation characteristics and novel structure.

Data Availability

The data used in this study are included in the figure files.

Conflicts of Interest

The authors declare that there are no conflicts of interest in this article.

Acknowledgments

This work was supported in part by the Natural Science Foundation of Hebei Province (No. F2021508009), the National Key R&D Project (No. 2020YFC1511805), Innovative Research Group Project of National Natural Science Foundation of China (No. 61821001), the Fundamental Research Funds for the Central Universities under grant 3142018048, and Education and Teaching Reform Special Project of NCIST (No. 1010403-71).

References

[1] Z. Yu, L Yao, Z. Lin, and X. Ran, "Design of window grille shape-based multiband antenna for mobile," *Terminal hindawi international journal of antennas and ropagation*, vol. 2021, Article ID 6684959, 14 pages, 2021.

[2] D.-G. Kang and Y. Sung, "Coupled-fed planar printed shorted monopole antenna for LTE/WWAN mobile handset applications," *IET Microwaves, Antennas & Propagation*, vol. 6, no. 9, pp. 1007–1016, 2012.

[3] Z. L. Xie, W. B. Lin, and G. L. Yang, "Coupled-fed printed antenna for LTE mobile handset applications," *Microwave and Optical Technology Letters*, vol. 56, no. 8, pp. 1752–1756, 2014.

[4] J. H. Chen, Y. L. Ban, H. M. Yuan, and Y. J. Wu, "Printed coupled-fed PIFA for seven-band GSM/UMTS/LTE WWAN mobile phone," *Journal of Electromagnetic Waves and Applications*, vol. 26, pp. 390–401, 2012.

[5] C. d. L. Nóbrega, M. R. da Silva, P. H. d. F. Silva, A. G. D'Assuncao, and G. L Siqueira, "Simple, compact, and multiband frequency selective surfaces using dissimilar sierpinski fractal elements," *International Journal of Antennas and Propagation*, vol. 20155 pages, Article ID 614780, 2015.

[6] Y. L. Ban, Y. F. Qiang, Z. Chen, K. Kang, and J. L. W. Li, "Lowprofile narrow-frame antenna for seven-band WWAN/LTE smartphone applications," *IEEE Antennas and Wireless Propagation Letters*, vol. 13, pp. 463–466, 2014.

[7] M. Borhani, P. Rezaei, and A. Valizade, "Design of a reconfigurable miniaturized microstrip antenna for switchable multiband systemsfigurable miniaturized microstrip antenna for switchable multiband systems," *IEEE Antennas and Wireless Propagation Letters*, vol. 15, pp. 822–825, 2016.

[8] J. S. Khinda, M. R. Tripathy, and D. Gambhir, "Multi-edged wideband rectangular microstrip fractal antenna array for C- and X-band wireless applications," *Journal of Circuits, Systems, and Computers*, vol. 26, no. 4, Article ID 1750068, 2017.

[9] W.-C. Weng and C.-L. Hung, "An H-fractal antenna for multiband applications," *IEEE Antennas and Wireless Propagation Letters*, vol. 13, pp. 1705–1708, 2014.

[10] N. T. Thanh, Y. Yang, K. Y. Lee, and K. C. Hwang, "Dual circularlypolarized spidron fractal slot antenna," *Electromagnetics*, vol. 37, pp. 40–48, 2017.

[11] Y. Braham Chaouche, I. Messaoudene, I. Benmabrouk, M. Nedil, and F. Bouttout, "Compact coplanar waveguide-fed reconfigurable fractal antenna for switchable multiband systems," *IET Microwaves, Antennas & Propagation*, vol. 138 pages, 2018.

[12] X. X. Yang, G.-N. Tan, B. han, and H. G. xue, "millimeter wave fabry-perot resonator antenna fed by CPW with high gain and broadband," *International Journal of Antennas and Propagation*, vol. 2016, Article ID 3032684, 7 pages, 2016.

[13] A. K. Gautam, L. Kumar, B. K. Kanaujia, and K. Rambabu, "Design of compact F-shaped slot triple-band antenna for WLAN/WiMAX applications," *IEEE Transactions on Antennas and Propagation*, vol. 64, no. 3, pp. 1101–1105, 2016.

[14] Z. Yu, Z. Lin, X. Ran, Y. Li, B. Liang, and X. Wang, "A novel "回" pane structure multiband microstrip antenna for 2G/3G/4G/5G/WLAN/navigation applications/4G/5G/WLAN/navigation," *International Journal of Antennas and Propagation*, vol. 2021, p. 1, Article ID 5567417, 2021.

[15] M. Naghshvarian Jahromi, A. Falahati, and R. M. Edwards, "Bandwidth and impedance-matching enhancement of fractal monopole antennas using compact grounded coplanar waveguide," *IEEE Transactions on Antennas and Propagation*, vol. 59, no. 7, pp. 2480–2487, 2011.

[16] A. Zaidi, W. A. Awan, N. Hussain, and A Baghdad, "A wide and tri-band flexible antennas with independently controllable notch bands for sub-6-GHz communication system," *Radioengineering*, vol. 29, no. 1, pp. 44–51, 2020.

[17] B. T. P. Madhav, P. Syamsundar, A. Ajay Gowtham, C. Vaishnavi, M. Gayatri Devi, and G. Sahithi Krishnaveni, "Elliptical shaped coplanar waveguide," *Feed Monopole Antenna" World Applied Sciences Journal*, vol. 32, no. 11, pp. 2285–2290, 2014.

[18] J. Anguera, C. Puente, C. Borja, and J. Soler, *Fractal-shaped Antennas:a Review*, K. Chang, Ed., vol. vol.2, Wiley, Wiley Encyclopedia of RF and Microwave Engineering, pp. 1620–1635, 2005.

[19] H. Oraizi and S. Hedayati, "Circularly polarized multibandmicrostrip antenna using the square and giuseppe peano fractals," *IEEE Transactions on Antennas and Propagation*, vol. 60, no. 7, pp. 3466–3470, 2012.